Zhe-Feng Zhang[a,b], Dieter Brunner[a], Christina Scheu[a,c], Manfred Rühle[a]

[a] Max-Planck-Institut für Metallforschung, Stuttgart, Germany
[b] Shenyang National Laboratory for Materials Science, Institute of Metal Research, Chinese Academy of Sciences, Shenyang, VR China
[c] Materialprüfungsanstalt, Universität Stuttgart, Stuttgart, Germany

Deformation and fracture mechanisms of Al_2O_3/Nb/Al_2O_3 composites under compression

The deformation and fracture behavior of polycrystalline Al_2O_3 and Al_2O_3/Nb/Al_2O_3 composites with perpendicular and inclined interfaces were investigated at room temperature by means of compression tests. It was found that polycrystalline Al_2O_3 fractured at higher stresses (>500 MPa) than Al_2O_3/Nb/Al_2O_3 composites, and that its failure always showed a split fracture mode. For the Al_2O_3/Nb/Al_2O_3 specimens with interfaces perpendicular to the loading direction, cracks normally nucleated near the Nb/Al_2O_3 interfaces and then propagated along the loading direction, finally leading to a split fracture in the polycrystalline Al_2O_3 parts. For the Al_2O_3/Nb/Al_2O_3 specimens with interfaces inclined to the loading direction, the split fracture of the polycrystalline Al_2O_3 parts strongly depends on the orientation of the Al_2O_3/Nb interfaces with respect to the loading direction. For all the Al_2O_3/Nb/Al_2O_3 specimens, intergranular cracking was seldom observed independent whether the interfaces are perpendicular or inclined to the loading direction. Based on these results, the fracture mechanisms of Al_2O_3 and Al_2O_3/Nb/Al_2O_3 specimens are discussed.

Keywords: Al_2O_3/Nb/Al_2O_3 composites; Compression, Interfaces; Split fracture

1. Introduction

Metal/ceramic interfaces are of major importance for many technological and industrial applications demanding advanced materials, including electronic packaging systems, thin-film technology, protective coating and structural metal/ceramic composites [1–3]. Therefore, the fracture behavior at metal/ceramic interfaces has received considerable attention since it is highly relevant to deformation and failure processes in elastic components and composite materials [4–8]. In the past two decades, the mechanical properties of metal/ceramic interfaces have been widely investigated by testing different Al/Al_2O_3 [9–13], Cu/Al_2O_3 [14–18], Au/Al_2O_3 [19–21], and Al_2O_3/Nb/Al_2O_3 [22–31] bicrystals or polycrystalline specimens. The goal of these studies was to determine the deformation and fracture mechanisms under various loading modes, for example, compact tension [11–17, 20, 21], compression [25, 26, 30, 31], bending [9, 19, 23, 28, 29, 31], fatigue [18], and indentation [22]. Normally, the fracture energies of the interfaces

between alumina and different metals are about several hundreds of J/m^2, being significantly higher than that of alumina [25, 26]. Recently, the fracture energy of Nb/α-Al_2O_3 interfaces was found to reach around ~ 2000 J/m^2, which is an extremely high value compared to the other systems mentioned above [28,29]. In particular, Nb and Al_2O_3 do not react chemically and have a similar thermal expansion coefficient [29], which can minimize the effect of residual thermal stress at the interfaces. Therefore, it is possible to deform the metal layer to a certain extent while maintaining the bonding at the Nb/α-Al_2O_3 interfaces, and thus to produce advanced metal/ceramic composites.

Early indentation tests in Al_2O_3/Nb/Al_2O_3 polycrystals showed that metal plasticity can be either beneficial due to plastic blunting of interface cracks, or detrimental because of residual stresses created around cracks in the ceramic [22]. Reimanis [23] deformed Nb/Al_2O_3 constituents with pre-cracks through in-situ bending tests. He observed the debonding of Nb/Al_2O_3 interfaces in-situ and a variance of the interface fracture energy due to the crystallographic orientation of the constituents. Soyez et al. [25,26] investigated the mechanical properties of sapphire/Nb/sapphire joints with different orientation relationships manufactured by diffusion bonding in ultra-high vacuum (UHV) by compression tests. They found that Young's modulus and yield stress of sapphire/Nb/sapphire joints were influenced by the thickness of the metal Nb layer. Recently, systematic tests showed that the interface fracture energy of Al_2O_3/Nb/Al_2O_3 joints strongly depends on the orientation relationship between Al_2O_3 and Nb and interfacial impurities [28, 29]. Higher fracture energy is caused by greater plastic deformation in the Nb layer through mount of slip lines on the metal fracture surfaces. For a better understanding of the deformation and fracture characteristics of the Nb/Al_2O_3 interfaces, a full-field optical strain measurement (OFM) technique was applied to record the surface deformation processes during compression and bending tests in sandwich-bonded joints of polycrystalline Al_2O_3/Nb/Al_2O_3 composites [30, 31]. However, all of the aforementioned tests did not show the deformation and fracture features in detail. In the present paper, polycrystalline Al_2O_3/Nb/Al_2O_3 joints with interfaces perpendicular or inclined to the loading direction are employed to observe their deformation and fracture features under compression loading, and to determine the influence of the interface inclination relative to the loading direction on the fracture behavior.
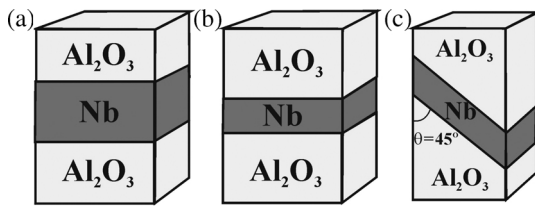
Fig. 1. Illustration of the $Al_2O_3/Nb/Al_2O_3$ specimens with interfaces perpendicular or inclined to the loading direction, and an Nb thickness of (a) 1.75 mm and (b) 0.92 mm. The specimens with interfaces inclined to the loading direction (c) have a thickness of 0.92 mm for the interfaces perpendicular to the loading direction and of 1.3 mm for the inclined interfaces.

2. Experimental Procedures

Polycrystalline niobium (purity 99.9 at.%) and alumina were employed for the bonding of $Al_2O_3/Nb/Al_2O_3$ composites. The Nb sheets, with a thickness range of $1-3$ mm, were received from Goodfellow, Germany. They were cut into a number of rectangular platelets and then ground and polished with a diamond suspension at both surfaces to a final thickness between 0.7 and 2.8 mm. The bonding process was performed at 1400 °C under a uniaxial pressure of 10 MPa for 3 hours in vacuum (10^{-6} Pa), followed by furnace cooling [30,31]. Then, the bonded $Al_2O_3/Nb/Al_2O_3$ samples were cut into different compressive specimens with dimensions of $3 \text{ mm} \times 3 \text{ mm} \times 6 \text{ mm}$, as shown in Fig. 1. There are two groups of $Al_2O_3/Nb/Al_2O_3$ specimens containing interfaces perpendicular to the loading direction and Nb layer thicknesses of 1.75 and 0.92 mm, respectively, as shown in Figs. 1a and b. The third group of $Al_2O_3/Nb/Al_2O_3$ specimens has interfaces which are either inclined to the stress axis with an angle of $\theta = 45°$ or perpendicular to the loading direction (Fig. 1c). The thickness of the Nb layer is also 0.92 mm, thus, corresponding to a height of 1.3 mm for the interfaces inclined to the stress axis direction. For comparison, polycrystalline Al_2O_3 specimens with the same dimensions were also machined. Before mechanical tests, all specimens were ground and polished carefully for surface observations. Some of the specimens were etched to reveal the Nb grains and then observed by electron backscatter diffraction (EBSD) technique to determine their orientation distribution. Compression tests were performed on a servo-mechanical testing machine (Zwick 1474) at room temperature. During testing, both the load and the displacement of the cross-head were recorded simultaneously by a linear variable displacement transducer (LVDT). The employed cross-head speed is 0.1 mm per minute. After compression, all the specimens were observed by a JSM6300-F scanning electron microscope (SEM) to reveal the deformation and fracture features.

3. Experimental Results

3.1. Orientations of Nb grains

The orientation distribution of the Nb grains in the $Al_2O_3/Nb/Al_2O_3$ specimens with interfaces perpendicular to the loading direction are shown in Figs. 2a–c. Along the loading direction of the specimens, the orientations of the Nb grains are close to the $\langle 111 \rangle$ direction (Fig. 2b); while the Nb grains along the normal direction of the surface are
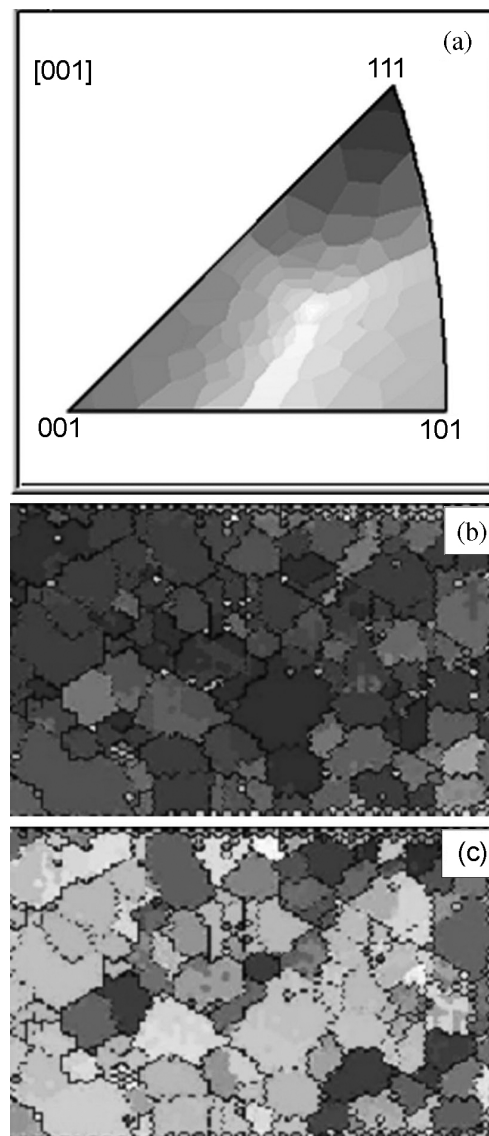

Fig. 2. Orientation distribution of the Nb grains in the specimen with interfaces perpendicular to the loading direction as measured by electron backscatter diffraction. (a) gives the stereographic triangle. The orientation images along the loading direction and the surface and the surface normal are displayed in (b) and (c).

randomly oriented and most of grain boundaries are large-angle ones (Fig. 2c). On the adjacent surface of the specimens, similar results were observed. The orientations of the Nb grains on the two adjacent surfaces of the $Al_2O_3/Nb/Al_2O_3$ specimens with interfaces inclined to the loading direction are shown in Fig. 3. There is no obvious texture on both surfaces containing perpendicular and inclined interfaces (see Figs. 3b and d). Besides, from Fig. 3c and e, it is apparent that most of the Nb grain boundaries are also of large-angle types. The Nb grain size in the three groups of specimens ranges from 100 to 200 μm, which is smaller than that (~ 500 μm) in the specimens investigated by Liu and Brunner [30] and Lin et al. [31].

3.2. Compressive stress – strain curves

Figure 4 shows the compressive stress–strain curves of Al_2O_3 and $Al_2O_3/Nb/Al_2O_3$ specimens with perpendicular interfaces. It can be seen that the polycrystalline Al_2O_3
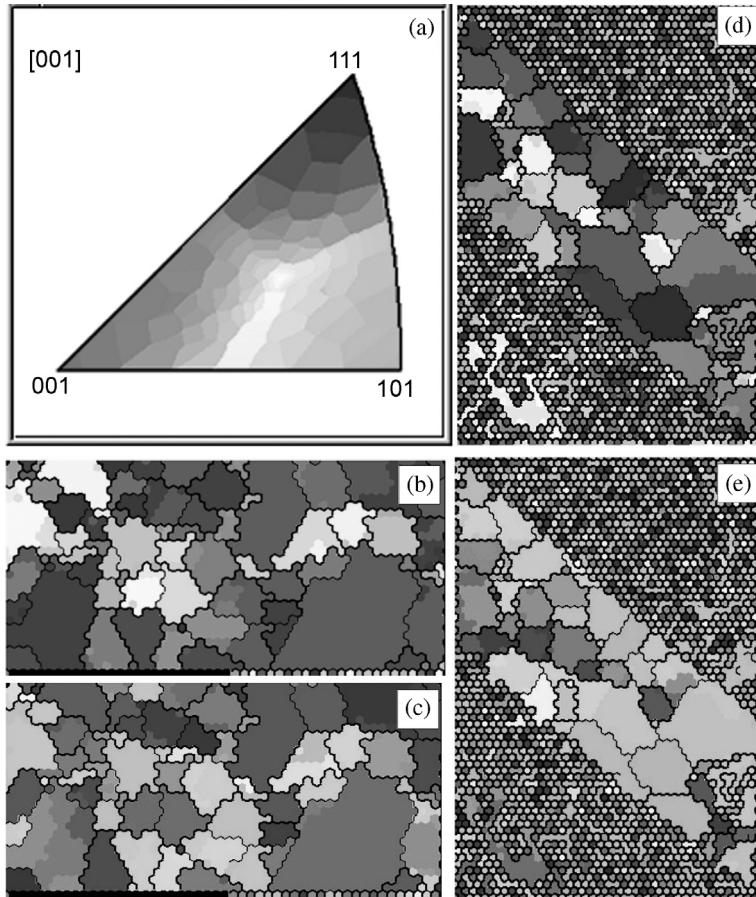
Fig. 3. Orientation distribution of the Nb grains in the specimen with interfaces inclined to the loading direction, as measured by electron backscatter diffraction. (a) reveals the stereographic triangle, (b) to (d) the grain orientation of surfaces containing perpendicular and inclined interfaces.

specimens only display elastic deformation and fail at a stress level of more than 500 MPa. The stress–strain curves of the $Al_2O_3/Nb/Al_2O_3$ specimens nearly overlap under both uniaxial and cyclic compression at low strain levels (below 2 %), as shown in Figs. 4a and b. However, at higher strain levels (above 2 %), the cyclic stress is slightly lower than the uniaxial compression stress (Fig. 4a). Figures 4c and d show the effect of the Nb thickness on the stress–strain curves of the $Al_2O_3/Nb/Al_2O_3$ specimens under uniaxial (Fig. 4c) and cyclic compression (Fig. 4d). The flow stress of the specimen with the smaller Nb thickness is always higher than that of the specimen with the larger Nb thickness.

The stress–strain curves of the $Al_2O_3/Nb/Al_2O_3$ specimens with interfaces inclined to the stress axis are shown in Figs. 5a and b. At a strain level below 3 %, the stress–strain curves of the $Al_2O_3/Nb/Al_2O_3$ specimen under uniaxial and cyclic compression also nearly overlap (Fig. 5a). At a strain range over 3 %, the flow stress under cyclic compression still has a lower value than that under uniaxial compression, which is consistent with the $Al_2O_3/Nb/Al_2O_3$ specimen with interfaces perpendicular to the loading direction. The shear stress, τ, resolved on the interface was calculated by $\tau = \sigma \sin\theta\cos\theta$, and the shear stress–strain curves are shown in Fig. 5b.

3.3. Observations of the deformation and fracture behavior

3.3.1. Polycrystalline Al_2O_3 specimens

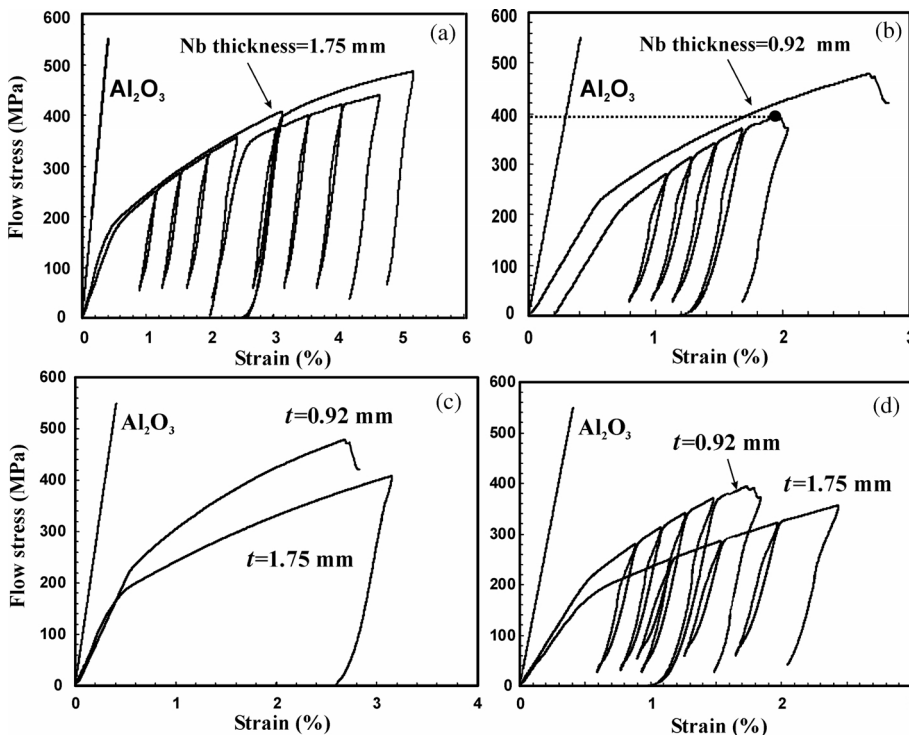The typical fracture behavior of polycrystalline Al_2O_3 specimens under compression is shown in

Fig. 4. Compressive stress–strain curves of polycrystalline Al_2O_3 and $Al_2O_3/Nb/Al_2O_3$ specimens with interfaces perpendicular to the loading direction and different Nb thicknesses (uniaxial and cyclic compression).

Figs. 6a and b, wherein the arrows indicate the loading direction. It is obvious that the fracture surfaces of the polycrystalline Al_2O_3 specimens are approximately parallel to the loading direction, which is typical for a split fracture mode. We have compressed more than 10 specimens and did not find any shear fracture. At some local sites of the fractured Al_2O_3 specimens, the large cracks are also mainly parallel to the stress axis direction (see Fig. 6c), indicating a split mode rather than a shear mode. This split fracture mode was frequently observed for some brittle materials, such as metallic glass composites with dendritic phases or tungsten fibers [32, 33], rocks [34] and polycrystalline ice [35].

3.3.2. $Al_2O_3/Nb/Al_2O_3$ with interfaces perpendicular to the loading direction

For the $Al_2O_3/Nb/Al_2O_3$ specimens with interfaces perpendicular to the loading direction, cracking and fracture were observed to occur first in the Al_2O_3 parts, parallel to the loading direction. Fig. 7a shows a deformed specimen with an Nb thickness of 0.92 mm at $\varepsilon_{pl} = 1.5\%$. A long crack has nucleated within one of the Al_2O_3 parts and is mainly parallel to the stress axis. From its stress–strain curve marked in Fig. 4b, the flow stress of the $Al_2O_3/Nb/Al_2O_3$ specimen is about 400 MPa, which is obviously lower than the fracture strength (> 500 MPa) of Al_2O_3 specimens. This

indicates that cracking of the Al_2O_3 part in $Al_2O_3/Nb/Al_2O_3$ specimens can occur at a lower stress level in comparison to Al_2O_3 specimens. At a higher strain level, the Nb layer in the $Al_2O_3/Nb/Al_2O_3$ specimen will undergo serious plastic deformation, as shown in Fig. 7b for an Nb layer thickness of 1.75 mm and in Fig. 7c for a Nb layer thickness of 0.92 mm. There are two cracks in the Nb layer and one large crack in the Al_2O_3 part for the specimen with an Nb thickness of 1.75 mm (Fig. 7b). In addition, the cracking in the Al_2O_3 part near the interface is relatively wide and becomes sharp towards outside, as indicated by the arrow. For the $Al_2O_3/Nb/Al_2O_3$ specimen with a Nb thickness of 0.92 mm, there are two large cracks in the Al_2O_3 part (see Fig. 7c). Both of the two cracks have a large displacement near the interface and propagate towards the lower end of the specimen. From these observations, it can be concluded that the cracking of the Al_2O_3 part first nucleates near the Al_2O_3/Nb interface and then propagates towards the surface of the specimens. Under large plastic strain, the typical failure of the $Al_2O_3/Nb/Al_2O_3$ specimens often shows a split fracture in the Al_2O_3 parts, accompanied with serious plastic deformation and failure within the Nb layer, as shown in Fig. 7d. The split fracture in the Al_2O_3 parts for the $Al_2O_3/Nb/Al_2O_3$ specimens is consistent with the failure mode of the polycrystalline Al_2O_3 specimens, and was also observed in other metal/ceramic joints [5, 26, 31].

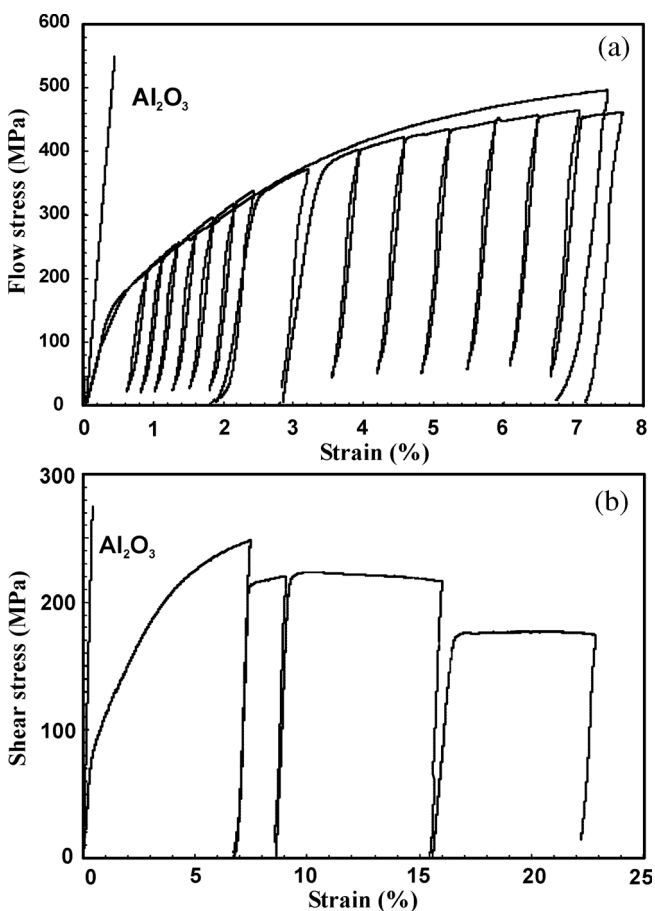Fig. 5. Compressive stress–strain curves of polycrystalline Al_2O_3 and $Al_2O_3/Nb/Al_2O_3$ specimens with interfaces inclined to the loading direction.
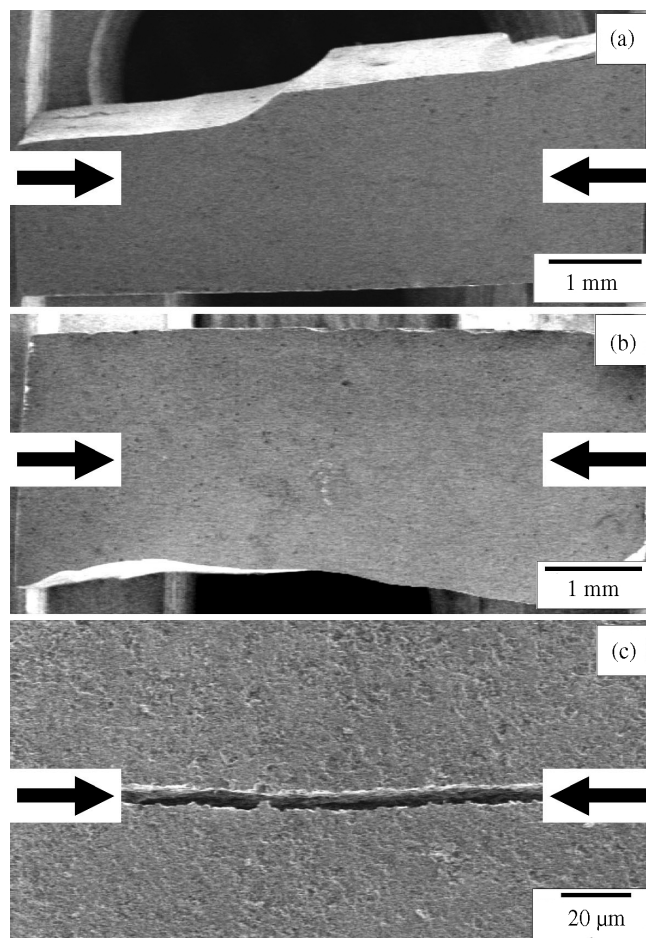
Fig. 6. Typical split fracture features of the polycrystalline Al_2O_3 specimens.

3.3.3. Al$_2$O$_3$/Nb/Al$_2$O$_3$ with interfaces inclined to the loading direction

For the Al$_2$O$_3$/Nb/Al$_2$O$_3$ joint with a metal layer inclined by 45° to the loading direction, interfaces which are inclined or perpendicular to the loading direction occur (geometry as shown in Fig. 1c). It is found that the cracking and fracture behavior of the Al$_2$O$_3$ parts strongly depends on the inter-

face orientation with respect to the loading direction. As shown in Fig. 8a, shear deformation of the Nb layer in the Al$_2$O$_3$/Nb/Al$_2$O$_3$ specimens can occur at $\varepsilon_{pl} = 1.5$ %, but no crack can be seen on the surface containing inclined interfaces. However, on the adjacent surface containing perpendicular interfaces a fine and slender crack appears in one of the Al$_2$O$_3$ parts, as indicated by the arrow in Fig. 8b. A small shear step has formed in the center of the Nb layer

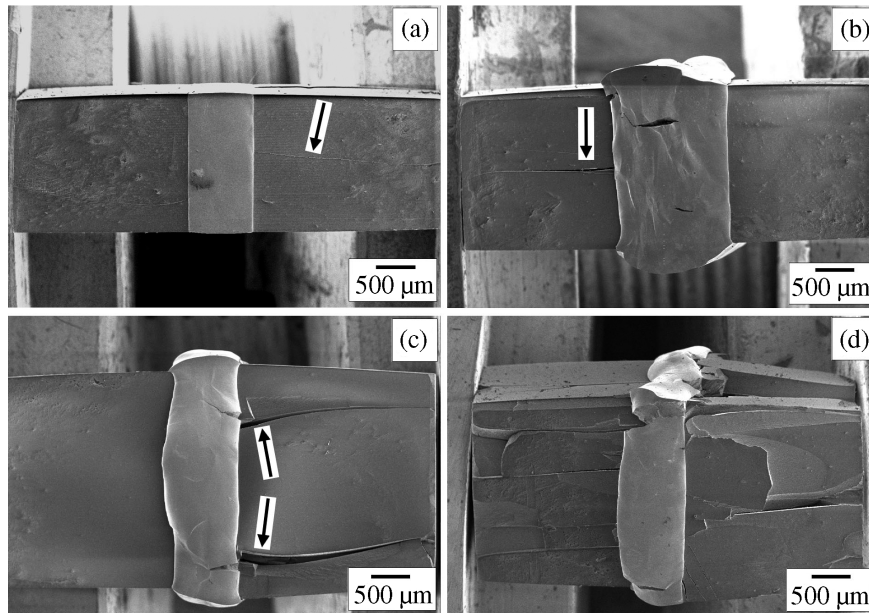Fig. 7. Typical macro-scale deformation and fracture of Al$_2$O$_3$/Nb/Al$_2$O$_3$ specimens with interfaces perpendicular to the loading direction. (a) $\varepsilon_{pl} = 1.5$ %, $t_{Nb} = 0.92$ mm; (b) $\varepsilon_{pl} = 2.5$ %, $t_{Nb} = 1.75$ mm; (c) $\varepsilon_{pl} = 6.5$ %, $t_{Nb} = 0.92$ mm; (d) $\varepsilon_{pl} = 16$ %, $t_{Nb} = 0.92$ mm. Arrows indicate location of cracks.
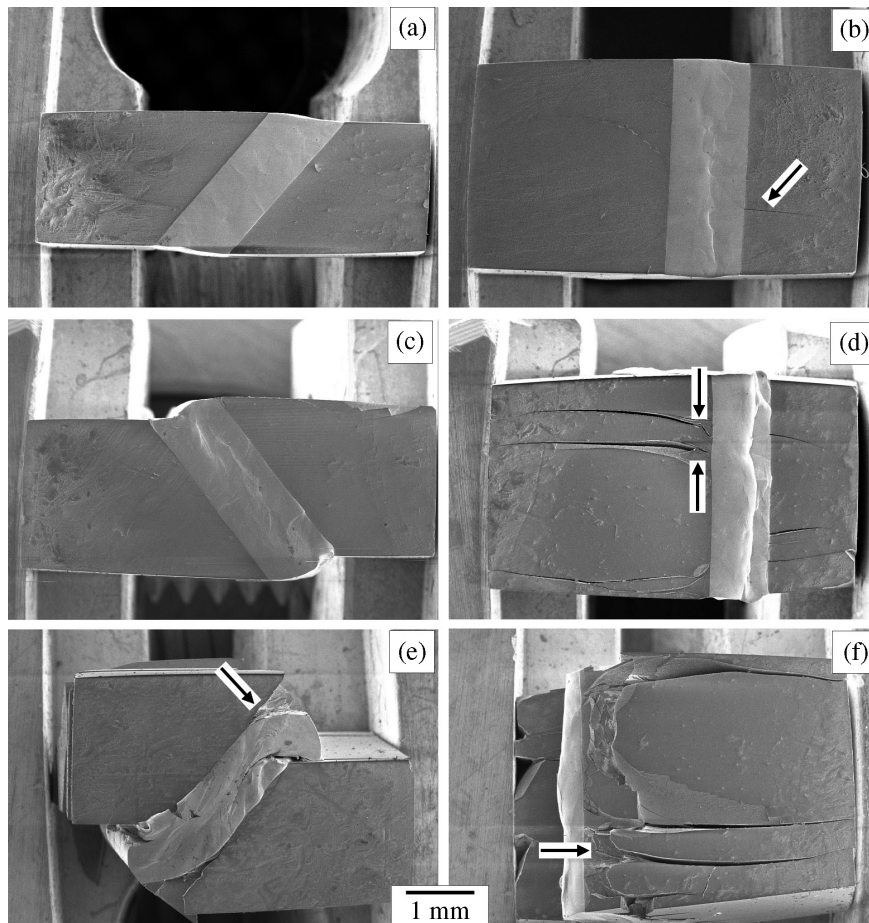
Fig. 8. Typical macro-scale deformation and fracture behavior on the surfaces of one Al$_2$O$_3$/Nb/Al$_2$O$_3$ specimen with both inclined and perpendicular interfaces. The strain is $\varepsilon_{pl} = 1.5$ % in (a) and (b). For (c) and (d) the strain is $\varepsilon_{pl} = 6.5$ %; and for (e) and (f) $\varepsilon_{pl} = 22$ %. Arrows indicate location of cracks.

due to the shear deformation. At $\varepsilon_{pl} = 6.5\%$, the specimen with inclined interface displayed strong shear deformation within the Nb layer (Fig. 8c). The two Al_2O_3 parts shift a relatively large distance, but there is still no crack on the surface containing the inclined interfaces. On the neighboring surface containing perpendicular interfaces (see Fig. 8d), the typical fracture mode is the cracking within the Al_2O_3 parts mainly parallel to the loading direction. Besides, the shear step of the Nb layer becomes more prominent, which is consistent with the observation on the adjacent surface of the inclined interfaces (see Fig. 8c). From the deformation morphology of the $Al_2O_3/Nb/Al_2O_3$ specimens, it is apparent that the cracking in the Al_2O_3 parts must originate from the interface first, then propagate towards outside up to the end of the specimen.

At $\varepsilon_{pl} = 22\%$, the deformation and fracture features can be seen in Figs. 8e and f. For the inclined interfaces, the relative shear displacement of the two Al_2O_3 parts reaches about 1.25 mm (Fig. 8e) which is nearly the same as the Nb thickness. However, the specimen did not separate along the interfaces after the large shear deformation. This indicates that the $Al_2O_3/Nb/Al_2O_3$ specimens can accommodate very large shear deformation and that the bonding of the Al_2O_3/Nb interfaces is strong. As shown in Fig. 8e, several local cracks appear within the Nb layer, leading to severe shear damage at this strain level. Besides this, the two Al_2O_3 parts still have no crack on the surface containing the inclined interfaces even at $\varepsilon_{pl} = 22\%$ (Fig. 8e). On the surfaces containing the perpendicular interfaces, the split fracture of the two Al_2O_3 parts becomes obvious, and many large cracks go through the whole Al_2O_3 parts (Fig. 8f). From the observations above, it can be concluded that for inclined interfaces cracking and split fracture of the Al_2O_3 parts are the main failure modes under compression, which is consistent with the polycrystalline Al_2O_3 specimens and the $Al_2O_3/Nb/Al_2O_3$ specimens with interfaces perpendicular to the loading direction. Another important feature is that at the surfaces containing inclined interfaces no crack nucleates even at very high strain levels (see Fig. 8e). On the contrary, on the surfaces containing only perpendicular interfaces cracks always form, even at a small strain (see Fig. 8b). This indicates that the cracking and split fracture of the Al_2O_3 parts in $Al_2O_3/Nb/Al_2O_3$ specimens strongly depend on the interface orientation relative to the loading direction. This will be analysed and discussed in the following Sections.
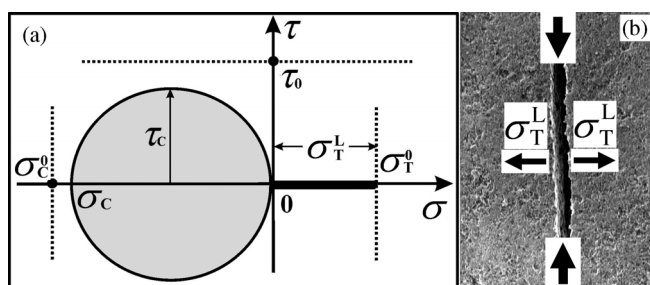

Fig. 9. (a) Illustration of the compressive stress distribution of the Al_2O_3 specimen on a Mohr circle along with the critical tensile fracture stress, σ_T^0, critical compressive fracture stress, σ_C^0 and shear fracture stress τ_0; (b) displays the split fracture and local lateral tensile stress σ_T^L of polycrystalline Al_2O_3 specimen under compression.
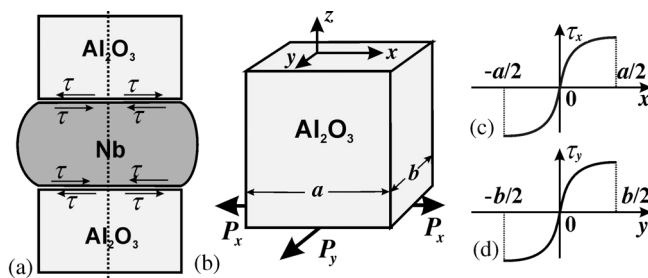
Fig. 10. (a) Illustration of a typical deformation mode of an $Al_2O_3/Nb/Al_2O_3$ specimen with interfaces perpendicular to the loading direction and shear stresses along the interfaces; (b) illustration of the tensile forces along x and y directions caused by the interface shear stresses for a specimen with dimension of $a \times b$; (c) and (d) illustration of the shear stress distribution along x and y directions.

4. Discussion

4.1. Fracture mechanism of polycrystalline Al_2O_3

Shear fracture has been frequently observed in many brittle materials, such as metallic glasses [33, 36, 37], polycrystalline ice [35], and nano-materials [38], and is often discussed using the Tresca criterion. As shown in Fig. 9a, if the maximum shear stress on any shear plane reaches a critical value τ_C, the materials fails in a shear mode, i. e.,

$$\tau_{max} = \sigma_{max}/2 \geq \tau_C \tag{1}$$

However, the polycrystalline Al_2O_3 specimens often fail in a split mode under compression, just as in some other brittle materials, such as metallic glassy composites containing steel fibers and dendritic phase [32, 33], rock [34] and polycrystalline ice [35]. It has been demonstrated that brittle glassy grain boundary phases often occur in commercial Al_2O_3 due to the sintering agents that are added to the material to facilitate densification during processing [39]. Thus, the brittle glassy grain boundary phases may fracture locally under shear resulting from compression. For a brittle material subjected to a compressive stress, σ_C, Goodier [40] proposed that the lateral tensile stress, σ_T^L, is related to σ_C by:

$$\sigma_T^L = \frac{3(1 + 5v)}{2(7 - 5v)}\sigma_C = K\sigma_C \tag{2}$$

Here, v is the Possion ratio of the material and is equal to $0.20-0.25$ for Al_2O_3; K can be regarded as a material constant and is equal to $0.50-0.60$ for Al_2O_3 [40]. It has been clarified that the remote compressive stress σ_C can cause, by virtue of microstructural inhomogeneities, localized regions of tension, which, in turn, leads to crack initiation [40]. The microstructural inhomogeneities that can nucleate cracks are mainly voids, grain boundaries, glassy grain boundary phases, and second-phase particles, around which tensile stresses are generated by compression [39]. Therefore, the existence of the lateral tensile stress σ_T^L is associated with the anisotropy of the brittle material and depends on the compressive stress σ_C. When σ_T^L is larger than the critical tensile fracture strength, σ_T^0, i. e.,
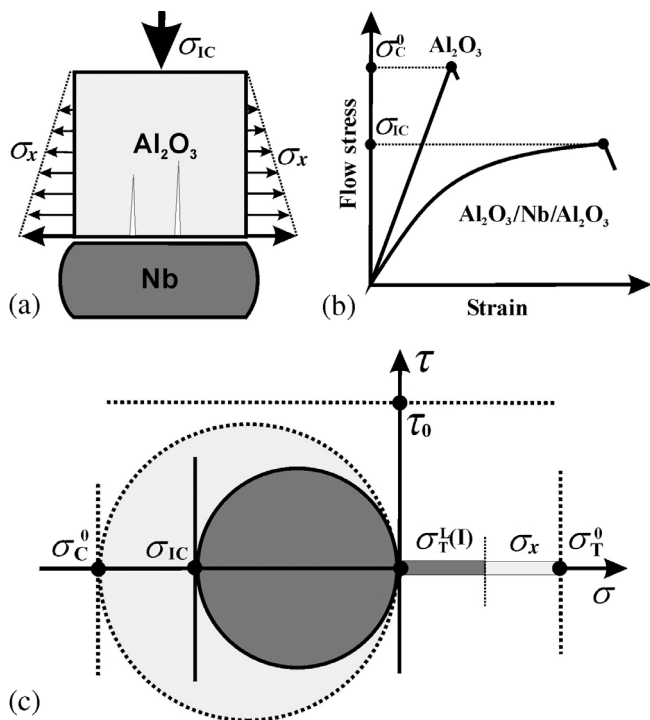
$$\sigma_T^L \geq \sigma_T^0 \tag{3}$$

Fig. 11. (a) Illustration of the nucleation of cracks within the Al_2O_3 part in an Al_2O_3/Nb/Al_2O_3 specimen with interfaces perpendicular to the loading direction and shear stress along the interfaces; (b) illustration of stress–strain curves of a polycrystalline Al_2O_3 and an Al_2O_3/Nb/Al_2O_3 specimen; (c) illustration of the compressive stress distribution on Mohr circles under the stresses σ_C and σ_{IC} and the critical tensile and shear fracture stresses.

the specimen will fail along the plane parallel to the loading direction, just as the tensile failure along the lateral direction, as shown in Fig. 9b. Therefore, a brittle material can fail either in a shear mode or in a split mode. For the polycrystalline Al_2O_3 specimens, split fracture is its intrinsic failure mode under compression.

4.2. Fracture mechanisms of Al_2O_3/Nb/Al_2O_3 specimens with interfaces perpendicular to the loading direction

From Fig. 4, it is apparent that a smaller Nb thickness leads to a higher flow stress, which is consistent with the results in Al_2O_3/Nb/Al_2O_3 tricrystals [25, 26] and polycrystals [30]. Since the orientation and grain size of the Nb layer are nearly the same for the two groups of specimens investigated in the present work, the difference in the flow stress can be mainly attributed to the effect of the Nb thickness, as discussed by Soyez et al. [25]. The split fracture of the Al_2O_3/Nb/Al_2O_3 specimens can occur at 200–400 MPa, which is lower than the fracture strength (>500 MPa) of the Al_2O_3 specimens. The occurrence of split fracture in the Al_2O_3 parts below the strength of the Al_2O_3 specimens reflects a strong effect of the Al_2O_3/Nb interfaces and will be discussed in more detail below.

If a compression load is applied to an Al_2O_3/Nb/Al_2O_3 specimen with interfaces perpendicular to the loading direction, the Nb layer will deform plastically, while the Al_2O_3 deforms elastically. At high strain levels, serious extrusions of the Nb layer can be seen at the specimen surfaces, as sketched in Fig. 10a. Consequently, the shear stress, τ, along the Nb/Al_2O_3 interfaces must be significant

during plastic deformation of the joint. The direction of the shear stress τ applied to the Al_2O_3 parts points towards outside; accordingly, the shear stress applied to the Nb layer points inside. For a rectangular Al_2O_3 specimen with dimensions of $a \times b$ (see Fig. 10b), there will be two shear stresses applied to the Al_2O_3 parts along x and y directions, i. e., τ_x and τ_y, respectively, following a function as shown qualitatively in Figs. 10c and d. Therefore, one can get additional tensile loads, P_x and P_y, along x and y direction, respectively, given as:

$$P_x = \int_0^{a/2} b \cdot \tau_x \, dx \tag{4a}$$

$$P_y = \int_0^{b/2} a \cdot \tau_y \, dy \tag{4b}$$

The two additional tensile loads P_x and P_y are produced by the interface shear stresses τ_x and τ_y during the strong plastic flow within the soft Nb layer. Furthermore, the distributions of the additional tensile stresses, σ_x and σ_y, applied to the Al_2O_3 parts can be illustrated as shown in Fig. 11a for σ_x. Obviously, the maximum stress of σ_x (or of σ_y) only appears near the interface.

On the other hand, it is known that the compression fracture strength, σ_C^0, of the Al_2O_3 specimens is always higher than 500 MPa, which corresponds to a split fracture. However, the split fracture of the Al_2O_3 parts in the Al_2O_3/Nb/Al_2O_3 specimens often occurs at a relatively low stress value. From their compressive stress–strain curves, it is apparent that the flow stress of the Al_2O_3/Nb/Al_2O_3 specimens is in the range of 200–500 MPa. The two stress–strain curves for the polycrystalline Al_2O_3 and the Al_2O_3/Nb/Al_2O_3 specimens are illustrated in Fig. 11b. From this, it can be deduced that the required flow stress, σ_{IC}, for the split fracture of the Al_2O_3 parts in an Al_2O_3/Nb/Al_2O_3 specimen is obviously lower than the compressive strength σ_C^0 of the polycrystalline Al_2O_3 specimens. The analysis given in Section 4.1 showed that the split fracture of the polycrystalline Al_2O_3 specimens can be attributed to the lateral tensile stress σ_T^L during compression. Therefore, this split fracture mechanism can be further applied to the Al_2O_3/Nb/Al_2O_3 specimens with perpendicular interfaces. The compressive stresses σ_c of polycrystalline Al_2O_3 and Al_2O_3/Nb/Al_2O_3 specimens in Fig. 11b can be deduced from the Mohr circles shown in Fig. 11c. The yellow Mohr circle represents the split fracture strength σ_C^0 of the Al_2O_3 specimen and can be expressed as:

$$\sigma_C \geq \sigma_C^0 \tag{5a}$$

or

$$\sigma_T^L = K\sigma_C^0 \geq \sigma_T^0 \tag{5b}$$

Here, σ_T^0 can be regarded as the tensile fracture strength of the Al_2O_3 specimen. For an Al_2O_3/Nb/Al_2O_3 specimen, the blue Mohr circle in Fig. 11c represents the critical stress σ_{IC} for the split fracture in the Al_2O_3 parts. Similar to Eq. (5b), the lateral tensile stress at an interface I, $\sigma_T^L(I)$, applied to the Al_2O_3 parts will be given as:

$$\sigma_T^L(I) = \frac{3(1 + 5v)}{2(7 - 5v)}\sigma_{IC} = K\sigma_{IC} \tag{6}$$

As shown in Fig. 4 and Fig. 11c, under a compressive stress σ_{IC}, it is known that

$$\sigma_{IC} < \sigma_C^0 \tag{7a}$$

or

$$\sigma_T^L(I) < \sigma_T^0 \tag{7b}$$

Consequently, the split fracture in the Al_2O_3 parts cannot occur if there is no effect of the Al_2O_3/Nb interfaces. However, as shown in Fig. 11a, there is an additional tensile stress, σ_x, applied to the Al_2O_3 parts due to the shear stress along the Al_2O_3/Nb interface. It is apparent that the additional tensile stress σ_x will promote the split fracture in the Al_2O_3 parts. If

$$\sigma_T^L(I) + \sigma_x \geq \sigma_T^0 \tag{8}$$

split fracture can also occur in the Al_2O_3 parts even at a lower compressive stress level of σ_{IC}. From Eqs. (5b), (6), and (8) it follows that if the split fracture begins to occur in the Al_2O_3 part, the following relationship is obtained:

$$K\sigma_{IC} + \sigma_x = K\sigma_C^0 \tag{9}$$

This explains why the split fracture stress σ_{IC} of the Al_2O_3 parts in an $Al_2O_3/Nb/Al_2O_3$ specimen is always lower than the split fracture strength σ_C^0 of the polycrystalline Al_2O_3 specimen. Furthermore, the difference between σ_C^0 and σ_{IC} can be expressed as:

$$(\sigma_C^0 - \sigma_{IC}) = \sigma_x/K \geq 0 \tag{10}$$

We have noted that the split fracture in the Al_2O_3 parts often originated from the Nb/Al_2O_3 interfaces, and then propagated towards the end of the $Al_2O_3/Nb/Al_2O_3$ specimen. This indicates that the maximum value of the additional tensile stress σ_x occurs near the Nb/Al_2O_3 interfaces, as illustrated in Fig. 11a. From the analysis above, it can be concluded that the split fracture of the Al_2O_3 parts in $Al_2O_3/Nb/Al_2O_3$ specimens is affected by both the lateral tensile stress $\sigma_T^L(I)$, caused by σ_{IC}, and the additional tensile stress σ_x (or σ_y), induced by the interface shear stress τ_x (or τ_y).

4.3. Fracture mechanisms of $Al_2O_3/Nb/Al_2O_3$ joints with interfaces inclined to the loading direction

From the observations provided in Fig. 8, it is apparent that the cracking and split fracture of the Al_2O_3 parts strongly depends on the Al_2O_3/Nb interface orientation with respect to the loading direction, an effect which has not been observed before. As illustrated in Fig. 12a, when a compressive load, P_0, is applied to the specimen, a shear stress τ_0 acts on the Nb/Al_2O_3 interface with

$$\tau_0 = (P_0/A_0) \cdot \sin\theta \cdot \cos\theta \tag{11}$$

As discussed in Section 4.2, there is also plastic flow and, therefore, extrusions of the Nb layer from the specimen surface occur (see Fig. 12a). Consequently, an additional interface shear stress, τ, will also act on both the Nb layer and Al_2O_3 parts during plastic deformation of the Nb layer, as sketched in Fig. 12a. For the Al_2O_3 parts, the distribution of the shear stress, τ_x, on the surfaces containing perpendicular interfaces should be symmetrical with respect to the x axis, as illustrated in Fig. 12b. In contrast, the shear stress, τ_y, on the surfaces containing inclined interfaces will give a shear-stress distribution due to the applied shear stress, τ_0, along the interface, as shown in Fig. 12c, which qualitatively is comparable with τ_x but is shifted by τ_0 in the τ_y direction. Similar to the discussion in Section 4.2, there should also exist additional tensile forces, P, on the different surfaces. Along the x direction, the values of the additional tensile forces, $P_{1,x}$ and $P_{2,x}$, are equal to each other and can be expressed as:

$$|P_{1,x}| = |P_{2,x}| = \int_0^{a/2} b^* \cdot \tau_x \, dx \tag{12}$$

Here, a and b^* are the width and the length of the cross-section, respectively. However, the values of the additional tensile forces $P_{1,y}$ and $P_{2,y}$ along the y direction are not in balance and can be expressed as:

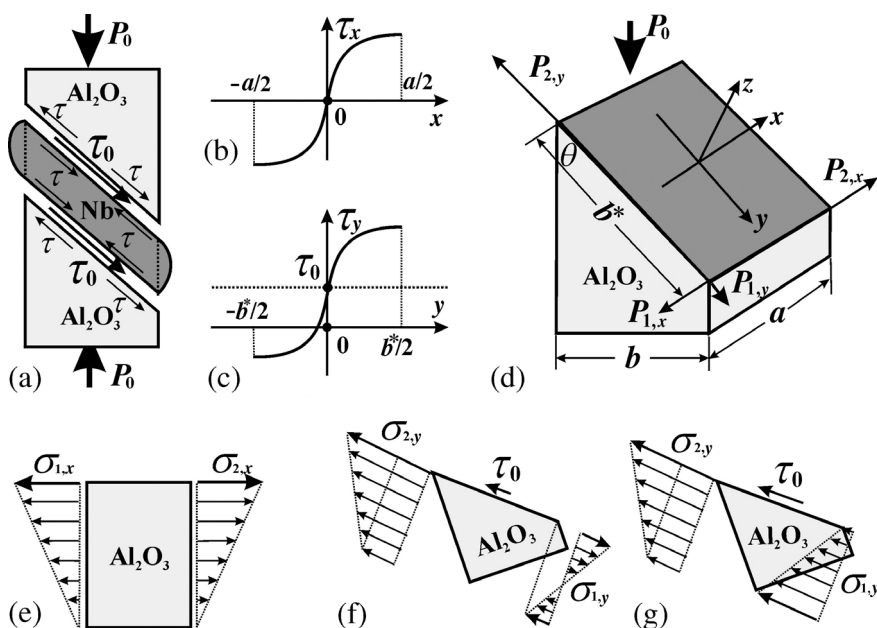$$|P_{1,y}| = \int_0^{b^*/2} a \cdot (\tau_y + \tau_0) \, dy \tag{13a}$$

Fig. 12. (a) Illustration of a typical deformation mode of the $Al_2O_3/Nb/Al_2O_3$ specimen with interfaces inclined to the loading direction, shear stress τ_0, and additional shear stresses along the interfaces; (b) and (c) show the shear stress distribution, respectively, along x and y directions on the interface plane; (d) displays the additional tensile forces $P_{1,x}$, $P_{2,x}$, $P_{1,y}$ and $P_{2,y}$ along x and y directions on the interface plane caused by the interface shear stress; (e) illustration of the additional tensile stresses $\sigma_{1,x}$ and $\sigma_{2,x}$ on the surfaces containing perpendicular interfaces; (f) and (g) displays the additional tensile stresses $\sigma_{1,y}$ and $\sigma_{2,y}$ on the surfaces containing inclined interfaces.

$$\left| P_{2,y} \right| = \int_0^{-b^*/2} a \cdot (\tau_y - \tau_0)\, \mathrm{d}y \tag{13b}$$

The additional tensile forces $P_{1,x}$, $P_{2,x}$, $P_{1,y}$ and $P_{2,y}$ are illustrated as in Fig. 12d. Furthermore, the additional tensile stresses $\sigma_{1,x}$, $\sigma_{2,x}$, $\sigma_{1,y}$ and $\sigma_{2,y}$ on the two surfaces can be illustrated as in Figs. 12e–g.

On the surfaces containing perpendicular interfaces, the additional tensile stresses $\sigma_{1,x}$ and $\sigma_{2,x}$ distribute symmetrically and the maximum tensile stress also occurs near the Nb/Al_2O_3 interfaces, as shown in Fig. 12e. Therefore, the split fracture mechanism on this surface will be similar to the one discussed in Section 4.2. However, the distribution of the additional tensile stresses $\sigma_{1,y}$ and $\sigma_{2,y}$ on the surfaces containing inclined interfaces will display two cases, as shown in Figs. 12f and g, depending on the relative value between τ_0 and τ_y. If $\tau_0 < \tau_y$, as shown in Fig. 12f, the direction of $\sigma_{1,y}$ and $\sigma_{2,y}$ should be opposite near the Nb/Al_2O_3 interface. In this case, the smaller additional tensile stress $\sigma_{1,y}$ plays a negligible role in the split fracture of the Al_2O_3 part on the surface containing inclined interfaces. If $\tau_0 > \tau_y$, the distribution of $\sigma_{1,y}$ and $\sigma_{2,y}$ can be illustrated as in Fig. 12g. This means that $\sigma_{1,y}$ and $\sigma_{2,y}$ act along the same direction and do not affect the split fracture of the Al_2O_3 part on the surface containing inclined interfaces. Since the Nb/Al_2O_3 interfaces have an angle of $45°$ with respect to the loading direction, the applied shear stress τ_0 reaches the maximum value along the interface. This might result in a distribution of $\sigma_{1,y}$ and $\sigma_{2,y}$ being more close to the case in Fig. 12g leading to the Al_2O_3 cracking on different surfaces, as observed in Fig. 8. The split fracture of the Al_2O_3 parts, thus, strongly depends on the interface orientation with respect to the loading direction.

5. Conclusions

From the experimental results above, the following conclusions can be made:

1. Polycrystalline Al_2O_3 specimens often fail in a split mode under compression, rather than in a shear mode. Its split fracture mode can be attributed to the lateral tensile stress σ_T^L due to the anisotropy in its microstructure.
2. For the $Al_2O_3/Nb/Al_2O_3$ specimens with perpendicular interfaces, split fracture was also observed in the Al_2O_3 parts. The crack first originated at the Nb/Al_2O_3 interfaces and then propagated towards the outside of the Al_2O_3 parts. The stress for split fracture of Al_2O_3 parts in $Al_2O_3/Nb/Al_2O_3$ specimens is lower than the split fracture strength of the polycrystalline Al_2O_3 specimens. The decrease in the split fracture stress can be attributed to the strong plastic flow of the Nb layer during compression, which produces an additional shear stress along the interfaces.
3. For the $Al_2O_3/Nb/Al_2O_3$ specimens with inclined interfaces, the split fracture in the Al_2O_3 parts shows a strong effect of the interface orientation relative to the loading direction. The split fracture always occurs on the two surfaces containing perpendicular interfaces, but does not take place on the neighboring surfaces containing inclined interfaces. The obvious difference in the split fracture feature on the two surfaces containing perpendicular and inclined interfaces can be attributed to the different stress distributions.

References

[1] F. Ernst: Mater. Sci. Eng. R14 (1995) 97.
[2] A.R. Wildes, J. Mayer, K. Theis-Brohl: Thin Solids Films 401 (2001) 7.
[3] N. Chandra, H. Li, C. Shet, H. Ghonem: Inter. J. Solids Struct. 39 (2002) 2827.
[4] M. Jokl, V. Vitek, C.J. McMahon, Jr.:, Acta Metall. 28 (1980) 1479.
[5] F.S. Shieu, R. Raj, S.L. Sass: Acta Metall. Mater. 38 (1990) 2515.
[6] H.M. Jensen: Acta Metall. Mater. 38 (1990) 2637.
[7] G.E. Beltz, J.R. Rice: Acta Metall. Mater., 40 (1992) 321.
[8] A.R. Akisanya, C.S. Meng: J. Mech. Phys. Solids 51 (2003) 27.
[9] H.C. Cao, A.G. Evans: Acta Metall. Mater. 39 (1991) 2977.
[10] A.G.. Evans, B.J. Dalgleish: Acta Metall. Mater. 40 (1992) S295.
[11] T. Akatsu, G. Sasaki, N. Hosoda, T. Suga: J. Mater. Res. 12 (1997) 852.
[12] O. Raddatz, G.A. Schneider, N. Claussen: Acta Mater. 46 (1998) 6381.
[13] I. Ziv, F. Weinberg, W.J. Poole: Scripta Mater. 40 (1999) 1243.
[14] G.E. Beltz, J.S. Wang: Acta Metall. Mater. 40 (1992) 1675.
[15] J.S. Wang: Acta Mater. 46 (1998) 4973.
[16] J.W. Kysar: Acta Mater. 48 (2000) 3509.
[17] P. Peralta, U. Ramamurty, S. Suresh, G.H. Campbell, W.E. King, T.E. Mitchell: Mater. Sci. Eng. A 314 (2001) 55.
[18] J.J. Kruzic, R.A. Marks, M. Yoshiya, A.M. Glaeser, R.M. Cannon, R.O. Ritchie: J. Am. Ceram. Soc. 85 (2002) 2531.
[19] I.E. Reimanis, B.J. Dalgleish, A.G. Evans: Acta Metall. Mater. 39 (1991) 3133.
[20] S.X. Mao, A.G. Evans: Acta Mater. 45 (1997) 4263.
[21] S.X. Mao, M.Z. Li: J. Mech. Phys. Solids 47 (1999) 2351.
[22] A.G. Evans, M.C. Lu, S. Schmauder, M. Rühle: Acta Metall. 34 (1986) 1643.
[23] I.R. Reimanis: Scripta Metall. 27 (1992) 1729.
[24] H. Ji, G.S. Was, M.D. Thouless: Eng. Fract. Mech. 61 (1998) 163.
[25] G. Soyez, G. Elssner, M. Rühle, R. Raj: Acta Mater. 46 (1998) 3571.
[26] G. Soyez, G. Elssner, M. Rühle: J. Mater. Sci. 35 (2000) 1087.
[27] J.X. Wu, V. Gupta: J. Mech. Phys. Solids 48 (2000) 609.
[28] D. Korn, G. Elssner, R.M. Cannon, M. Rühle: Acta Mater. 50 (2002) 3881.
[29] R.M. Cannon, D. Korn, G. Elssner, M. Rühle: Acta Mater. 50 (2002) 3903.
[30] Y. Liu, D. Brunner: Z. Metallkd. 93 (2002) 444.
[31] Y. Liu, C. Kohnle, D. Brunner, M. Rühle: Z. Metallkd. 94 (2003) 694.
[32] K.Q. Qiu, A.M. Wang, H.F. Zhang, B.Z. Ding, Z.Q. Hu: Intermetallics 10 (2002) 1283.
[33] Z.F. Zhang, G. He, J. Eckert, L. Schultz: Phys. Rev. Lett. 91 (2003) 4550501.
[34] Z.X. Zhang, J. Yu, S.Q. Kou, P.A. Lindqvist: Int. J. Rock Mech. Min. Sci. 38 (2001) 211.
[35] I.J. Jordaan: Eng-Fract. Mech. 68 (2001) 1923.
[36] P.E. Donovan: Acta Mater. 37 (1989) 445.
[37] W.J. Wright, R. Saha, W.D. Nix: Mater. Trans. 42 (2001) 642.
[38] Q. Wei, D. Jia, K.T. Ramech, E. Ma: Appl. Phys. Lett. 87 (2002) 1240.
[39] M.A. Meyers, R.W. Armstrong, H.O.K. Kirchner: Mechanics and Materials, John Wiley Sons, INC, 1999.
[40] N. Goodier: J. Appl. Mech. 1 (1993) 39.

Correspondence address

Dr. Zhe-Feng Zhang
Shenyang National Laboratory for Materials Science
Institute of Metal Research, Chinese Academy of Sciences
Shenyang, 110016, P. R. China
Tel.: +86 24 2397 1043
Fax: +86 24 2389 1320
E-mail: zhfzhang@imr.ac.cn